Microneedle array-based electrochemical sensor functionalized with SWCNTs for the highly sensitive monitoring of MDMA in interstitial fluid

Ana-Maria Dragan[a,b], Marc Parrilla[b,c*], Sofie Cambré[d], Juan Domínguez-Robles[e,f], Usanee Detamornrat[e], Ryan F. Donnelly[e], Radu Oprean[a], Cecilia Cristea[a], Karolien De Wael[b,c*]

[a] *Department of Analytical Chemistry, Faculty of Pharmacy, 'Iuliu Haţieganu' University of Medicine and Pharmacy Cluj-Napoca, Pasteur 6, 400349 Cluj-Napoca, Romania*

[b] *A-Sense Lab, University of Antwerp, Groenenborgerlaan 171, 2010 Antwerp, Belgium*

[c] *NANOlab Center of Excellence, University of Antwerp, Groenenborgerlaan 171, 2010 Antwerp, Belgium*

[d] *NANOrOPT, Department of Physics, University of Antwerp, Universiteitsplein 1, 2610 Antwerp, Belgium*

[e] *School of Pharmacy, Medical Biology Centre, Queen's University Belfast, 97 Lisburn Road, Belfast BT9 7BL, United Kingdom*

[f] *Department of Pharmacy and Pharmaceutical Technology, University of Seville, 41012 Seville, Spain*

*Corresponding author: Marc Parrilla (marc.parrillapons@uantwerpen.be), Karolien De Wael (karolien.dewael@uantwerpen.be); A-Sense Lab, Bioscience Engineering Department, University of Antwerp, Groenenborgerlaan 171, 2020, Antwerp, Belgium.

Highlights

- A microneedle (MN) array-based electrochemical platform was fabricated.
- A hollow MN patch was successfully integrated into a wearable electrochemical sensor.
- The enhancement of the MDMA signal using nanomaterials on the MN was achieved.
- The performance of the sensor is reported in buffer and artificial interstitial fluid.

Abstract

Illicit drug consumption constitutes a great concern worldwide due to its increased spread and abuse, and the negative consequences exerted on society. For instance, 3,4-methylenedioxymethamphetamine (MDMA), a synthetic amphetamine-type substance, was abused by 20 million people worldwide in 2020. This psychoactive substance exerts a myriad of effects on the human body being dangerous for the consumer's health. Besides, MDMA has been used in the treatment of some psychiatric conditions. Therefore, the development of wearable devices for MDMA sensing in biological fluids is of great importance for forensic toxicology (e.g., monitoring of patients with suspected or known MDMA consumption) as well as for therapeutic management of patients. Herein, we report the development of a wearable electrochemical platform based on a hollow microneedle (MN) array-based sensor for the monitoring of MDMA in the interstitial fluid by square-wave voltammetry. First, the holes of the MN array were modified with conductive pastes to devise a MN patch with a three-electrode system. Subsequently, the functionalization of the working electrode with nanomaterials enhanced MDMA detection. Thereafter, analytical parameters were evaluated exhibiting a slope of 0.05 μA μM^{-1} within a linear range from 1 to 50 μM and a limit of detection of 0.75 μM in artificial interstitial fluid. Importantly, critical parameters such as selectivity, piercing capability, temperature, reversibility and stability were assessed. Overall, the obtained MN sensor exhibited excellent analytical performance, making it a promising tool for MDMA tracking in interstitial fluid for individuals on probation or under therapeutic treatment.

Graphical abstract

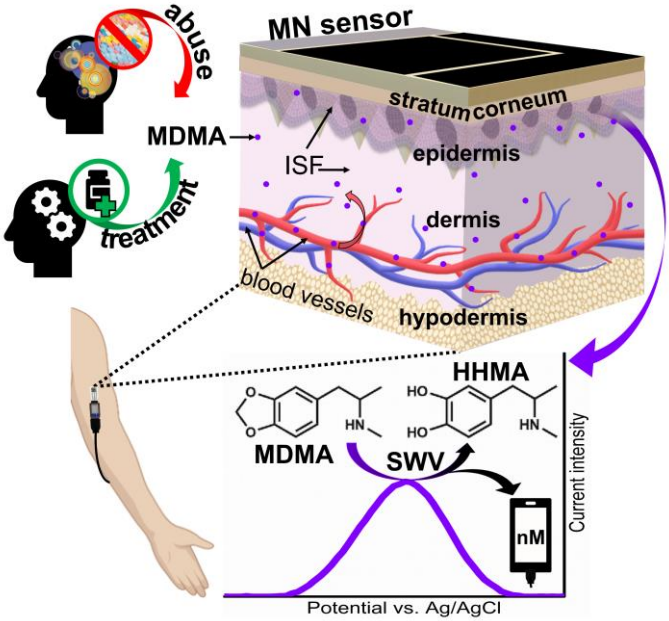

Key words:
wearable electrochemical sensor; microneedle array; forensic analysis; interstitial fluid; drugs of abuse; carbon nanotubes.

1. Introduction

3,4-Methylenedioxymethamphetamine (MDMA) is an amphetamine-type illicit drug, presently classified as a Schedule I drug [1,2]. According to the most recent report of the United Nations Office on Drugs and Crimes (UNODC), around 20 million users were consuming MDMA globally in 2020 [3]. The frequent abuse of MDMA can be attributed to its psychoactive effects such as euphoria, hallucinations, and higher-order cognitive processing. Nevertheless, MDMA users are exposed to a myriad of negative consequences on their health such as cardiovascular anomalies (tachycardia and hypertension), cognitive impairment (i.e., memory loss, response inhibition), convulsions, insomnia, paranoia, and many others [1,4]. Traditionally, in clinical drug testing, the assessment of illicit drugs consumption is performed by presumptive tests (i.e., colorimetric tests and immunoassays) for screening in urine, plasma, or saliva, usually followed by a confirmation test using chromatographic techniques coupled to (tandem) mass spectrometry which is the gold standard technique in the forensic analysis [1,5].

The (potentially) portable sensing of MDMA has been reported for some biological matrices [1] such as serum, urine [6,7], saliva, or fingerprints [8] employing surface-enhanced Raman spectroscopy. Another intriguing strategy was reported by *Pollard et al.* which described the development of a point-of-care test for the detection of MDMA in latent fingerprints using surface plasmon resonance and lateral flow immunoassay technologies. The sample required no pretreatment and exhibited excellent performance in sensitivity, specificity and accuracy parameters (100%, 95% and 98%, respectively) [8].

Electrochemical methods were intensively used as portable alternatives for MDMA detection in biofluids, using either unmodified electrodes [9,10] or platforms functionalized with various structures such as antibodies [11], molecularly imprinted polymers [12] or metallic and carbonaceous nanomaterials [13]. The analysis of MDMA in spiked serum samples was achieved by *Garrido et al.* using a glassy carbon electrode and voltammetry as the analytical technique. However, the obtained limit of detection (LOD) was 2.4 µM which is above the reported peak concentrations of MDMA in plasma (0.7 µM - 1.15 µM [14]) [15]. Alternative matrices such as saliva and urine have been used for the electrochemical detection of MDMA. For example, bare carbon SPEs were employed for MDMA detection in saliva by mixing the sample with either a buffer solution [9] or with a surfactant-mediated solution [10], the latter displaying enhanced analytical performance. In another work, an amperometric immunosensor was developed for the highly specific and sensitive detection of MDMA in saliva and urine, outperforming the ELISA methods, but with a very long incubation time (45 min) [11]. Another approach proposed by *Couto et al.* consisted of using a molecularly imprinted polymer-based sensor for the analysis of MDMA using voltammetry. The sensor was applied for the screening of serum and urine samples with LODs of 3.9 µM and 6.4 µM, respectively, using an incubation time of 10 min [12]. More recently, carbon nanohorns decorated with platinum nanoparticles were employed for the development of a highly sensitive electrochemical sensor using differential pulse voltammetry, reaching a LOD of 0.018 µM in buffer. However, when the sensor was applied for the analysis of spiked serum and urine samples, the lowest analyzed concentration was 0.5 µM for both samples [13].

An attractive alternative for the identification and monitoring of illicit drug abuse is the use of wearable devices, for which an increasing trend of use was observed in healthcare assistance [16–18]. Given the negative consequences illicit drug abuse exerts on human health and society, it is not surprising that some advances were reported for the development of wearable devices for the detection of illicit drugs [19]. Among these are several electrochemical devices, which constitute an emerging technology in forensic analysis due to their excellent analytical capabilities, low cost, and user-friendliness [1]. Intriguing examples include a ring for tetrahydrocannabinol sensing in saliva [20], gloves for cocaine [21] and fentanyl [22] screening in street samples, and a microneedle (MN) array for opioids (morphine and norfentanyl)

detection in interstitial fluid (ISF) [23]. The majority of reported wearable electrochemical sensors for drug analysis employ voltammetry (e.g., square-wave voltammetry or differential pulse voltammetry) as it allows a fast analysis of the sample without any complex treatments. This is only meaningful when the analyte of interest is electroactive in the working potential window of the electrode at specific conditions (e.g., pH) of the sample. In this case, the electrochemical profiling allows the identification of the analyte according to its oxidation potential. The rapid profiling avoids the use of recognition elements labelled with electroactive molecules (e.g. aptamers) or other labelling steps in which the electrode needs to be washed and incubated (e.g., when using antibody conjugated strategies).

Another important aspect is that several clinical studies were reported for the approval of some currently classified illicit drugs (i.e., psilocybin, lysergic acid, MDMA and ayahuasca) to be used in the treatment of several psychiatric conditions [24,25]. For instance, MDMA is being evaluated in the treatment of obsessive-compulsive disorder (OCD) [26], anxiety [27,28] and post-traumatic stress disorder (PTSD) [29,30], the latter being already approved in Australia by the Therapeutic Goods Administration [31]. Therefore, the development of wearable devices for MDMA identification and monitoring in biological fluids is of great importance for forensic toxicology within the range of interest, i.e. 0.24 µM and 2.41 µM [32–34], as well as for the proper management of the patients under MDMA treatment. Potential applications include identification and monitoring of patients with suspected or known MDMA consumption, cases of suspected overdose or abstinence monitoring.

MN arrays represent an emerging platform for the development of wearable electrochemical sensors, being able to penetrate the stratum corneum barrier (the top layer of the epidermis) and reach the ISF, the biofluid present in the dermis layer. ISF can serve as a biological matrix for minimally invasive monitoring of the health status as well as the substance intaking, including abused illicit drugs, since the species present in blood pass in the ISF by diffusion through the walls of the blood capillaries present in the dermis [35,36]. Hence, MN array platforms can be used for the identification and monitoring of different target species present within this biological fluid [37–39], of which concentration can be correlated with the levels in blood [40]. For the fabrication of MN-based sensors, two types of MN arrays can be used: solid and hollow MN arrays (HMN) [40,41]. The latter can be employed in different manners for the development of an electrochemical sensor, such as the attachment of the HMN array to screen-printed electrodes (SPEs) [41,42], the insertion of the electrochemical cell into the HMN [43,44], or the filling of the HMN with conductive pastes [45,46].

MDMA was chosen as the target since its concentration in blood, and consequently in ISF, is reportedly higher than that of its metabolites [32–34,47]. Firstly, an optimization study was conducted to ensure the suitability of the electrochemical sensor for MDMA analysis in ISF. Hence, a variety of nanomaterials were investigated for the enhancement of the MDMA electrochemical signal, since this has been proved useful in previous works [48,49]. The included nanomaterials were either carbon-based, i.e., single-walled carbon nanotubes (SWCNTs), graphene oxide (GO) and nanodiamond particles (nDs), or metallic nanoparticles, i.e., gold nanoparticles (AuNPs) and palladium nanoparticles (PdNPs). The MN sensor performance was investigated in buffer and artificial ISF (AISF) to prove its suitability for the intended purpose. Hence, the linear range, LOD and limit of quantification (LOQ) were determined. Additionally, the selectivity of the sensor was investigated against common species found in biofluids (i.e., tyrosine, glycine, ascorbic acid and uric acid [41]) and other possible interferents such as: (i) commonly abused illicit drugs from the class of the synthetic cathinones (butylone and 3-methylmethcathinone), opioids (heroin and morphine) and cocaine [3]; (ii) illicit drugs metabolites (morphine and benzoylecgonine, as metabolites of heroin and cocaine [50–52], respectively), and (iii) frequently encountered adulterants (caffeine and paracetamol [53]). Importantly, critical parameters that might influence the performance of the sensor were further investigated by performing a Parafilm M® piercing test [54], a temperature study, and reversibility and stability tests.

To the best of our knowledge, no wearable devices were reported to date for the detection of MDMA in ISF. Hence, we report herein for the first time the fabrication and analytical evaluation of a wearable electrochemical sensor based on a HMN patch filled with conductive

pastes and functionalized with SWCNTs for the electrochemical identification and monitoring of MDMA by square-wave voltammetry (SWV) in ISF (**Fig. 1a**).

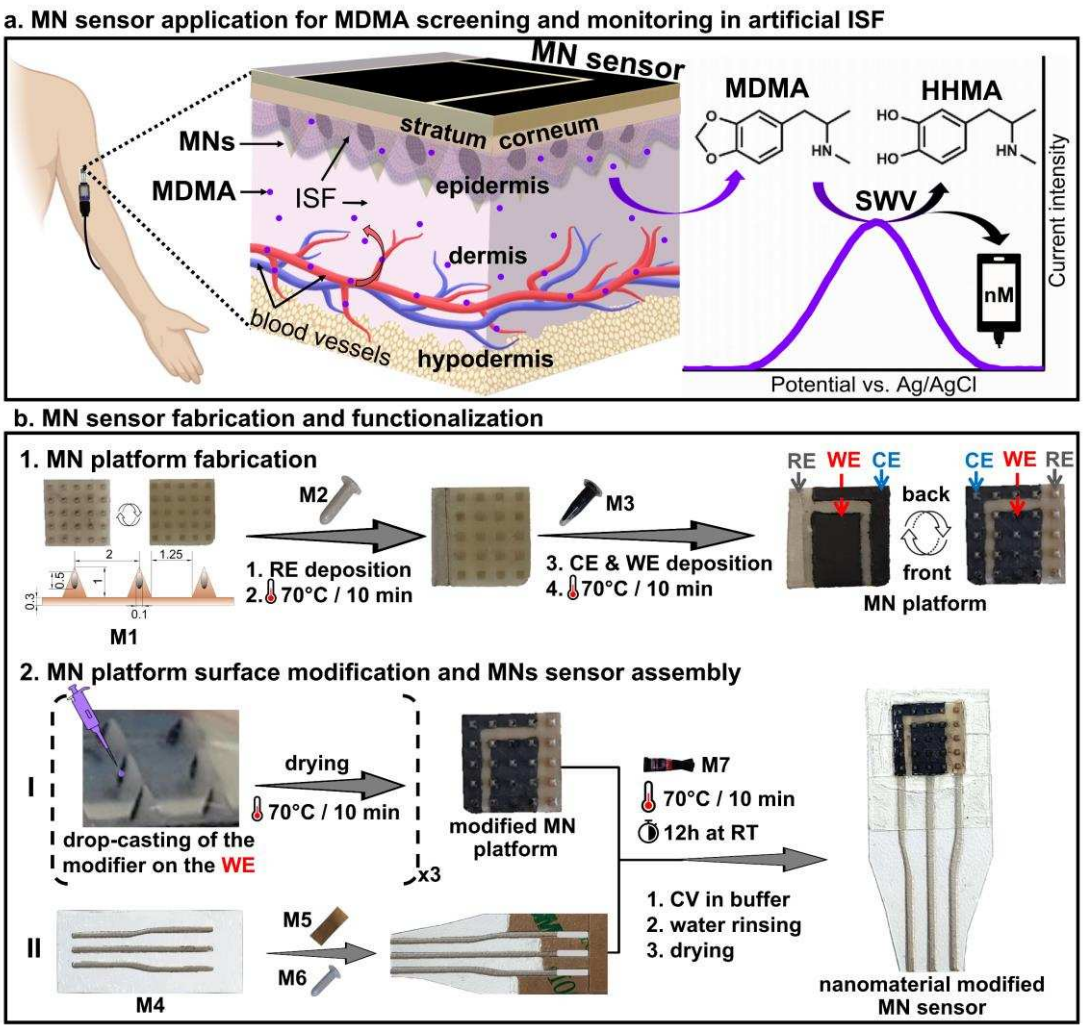

Fig 1. ***a)*** *The concept of MDMA identification and monitoring in ISF using the MN sensor.* ***b)*** *Schematics of the MN platform fabrication (b1), functionalization (b2.I) and assembly of the sensor (b2II) using a hollow microneedle array (M1*; dimensions in mm*), Ag/AgCl paste (M2), graphite paste (M3), screen-printed connections (M4), double adhesive tape (M5), silver paste (M6) and glue (M7). HHMA: 3,4 - dihydroxy-methamphetamine; RE: reference electrode; WE: working electrode; RT: room temperature; CV: Cyclic Voltammetry. The bioelements (arm and skin components) were generated using Biorender.*

2. Materials and methods

2.1 Materials and reagents

The standards of MDMA hydrochloride (HCl), 3-methylmethcathinone HCl, butylone HCl, cocaine HCl, heroin HCl, and morphine HCl were purchased from Lipomed, Switzerland and Chiron AS, Norway. The standards of ascorbic acid, caffeine, glycine, paracetamol, sodium dodecyl sulfate (SDS), tyrosine, and uric acid were purchased from Sigma-Aldrich (Overijse, Belgium). Palladium powder, graphene oxide solution (2 mg mL $^{-1}$) and nanodiamond particle dispersion (10 mg mL $^{-1}$) were purchased from Sigma Aldrich (Overijse, Belgium). The gold nanoparticles solution was prepared from gold (III) chloride trihydrate and sodium citrate (purchased from Sigma-Aldrich), according to the method reported by *Mendonca et. al* [55]. SWCNTs synthesized by the arc-discharge method (diameter 1.4 ± 0.2 nm) and subsequently

purified by air oxidation by Carbon Solutions Inc (P2, batch #03-A019) were solubilized by adding 2.5 mg mL $^{-1}$ of the SWCNTs to a 1% wt/V solution of SDS (Acros Organics, 99%) in deuterated water (D_2O, Cortecnet, 99.8 atom%D). The solutions were sonicated for 30 minutes in a bath sonicator (BRANSONIC,1510E-MTH) and then stirred on a magnetic stirring plate for 2 months. Afterward, medium-speed centrifugation was applied (4 h at 16 215 g with a tabletop centrifuge Sigma 2-16KCH in a swing-out rotor), and the supernatant was collected for further sensor development. Absorption spectra of the obtained SWCNTs solution were obtained in a Cary5000 UV-vis-NIR absorption spectrometer using a quartz microcell (60uL) with a path length of 3 mm.
ItalSens SPEs with a graphite working electrode (WE) (Ø = 3 mm), a carbon counter electrode (CE) and a silver pseudo-reference electrode (RE) were purchased from PalmSens, (The Netherlands) and were used for the platform and waiting time optimization.
Conductive pastes of silver/silver chloride (Ag/AgCl) and graphite (Sun Chemicals) purchased from Dupont Limited, UK., and hollow microneedle arrays (consisting of 5 x 5 pyramidal HMNs) were used to manufacture the MN electrochemical platform. The HMN patches were fabricated from polyether ether ketone (PEEK) sheets which were machined using a nanosecond-pulse, diode-pumped, solid-state laser operating. The dimensions and evaluation of the piercing capability are described in our previous works [41,56]. Silver paste purchased from Sun Chemicals, UK, was used to manually screen-print the connections for the MN platform on a polyethylene terephthalate (PET) substrate (125 µm). Double adhesive tape and glue were used for the assembly of the MN sensors.
Phosphate buffer saline (PBS) solution of 20 mM with 100 mM KCl and pH 7.4 was prepared using analytical grade dipotassium hydrogen phosphate, potassium dihydrogen phosphate (NaH_2PO_4), potassium chloride (KCl) and potassium hydroxide purchased from Sigma-Aldrich (Overijse, Belgium).
Artificial interstitial fluid at pH 7.4 was prepared in water according to a previously reported recipe [41,57] using 4-(2-hydroxyethyl)-1-piperazineethanesulfonic acid (HEPES), calcium chloride ($CaCl_2$), KCl, magnesium chloride ($MgCl_2$), NaH_2PO_4 and sodium chloride (NaCl), purchased from Sigma-Aldrich (Overijse, Belgium).
All solutions were prepared in 18.2 MΩ cm^{-1} doubly deionized water (Milli-Q water systems, Merck Millipore, Germany).

2.2 Methods and instrumentation

2.2.1 Instrumentation and electrochemical methods

Experiments requiring a temperature-controlled environment were performed inside a Mistral heater (Spark Holland B.V., the Netherlands).
A pH-meter (914 pH/Conductometer, 2.914.0020, Metrohm, Switzerland) was used to measure the pH whenever it was needed.
The Silhouette Cameo cutter (USA) was employed to design and cut the shape of the connections on a PET substrate which was used for screen-printing the connections.
All electrochemical experiments were performed using the MultiPalmSens4 potentiostat (PalmSens, The Netherlands) operated with the PSTrace 5.9 software. Cyclic voltammetry (CV) was employed for the preliminary electrochemical study of MDMA on the MN sensor (see *Section 2.2.3*). SWV (from 0.3 V to 1.2 V, with a step of 5 mV, an amplitude of 25 mV, a frequency of 10 Hz and 5 s equilibration time) was employed for the optimization and analytical characterization of the MN sensor. For better visualization, all SWVs were baseline-corrected using the “moving average baseline” option (window size: 2 points) available in the PSTrace 5.9 software. The data analysis and graphs representation were performed using the OriginPro 8.5 software (OriginLab, United States). The chemical structures were generated using the ChemDraw tool.

2.2.2. Method optimization

Before using the MN sensor, two parameters were investigated on SPEs: (i) the functionalization with nanomaterials of the WE and (ii) the waiting time (adsorption time of the

analyte) before analysis. Firstly, the signal of a 10 µM MDMA solution in PBS (pH 7.4) was registered by SWV on SPEs, either bare or modified with various nanomaterials: SWCNTs, rGO, nD, AuNPs and PdNPs. The influence of the SDS surfactant over the MDMA signal was investigated as well since the SWCNTs and rGO solutions were prepared with surfactants. The SPEs modification protocols are described in the supplementary material, namely the *Modification protocols of SPEs with nanomaterials*, in the "**Methods**" section.
The waiting time before analysis, defined as the time that passed between the moment in which the MN sensor was put in contact with the interrogated solution and the start of the SWV test, was further investigated. For this, SPEs modified with the best performing two candidates among the tested nanomaterials were used. Hence, the signal of MDMA was registered on the bare and nanomaterial-modified SPEs at 0.0, 1.0, 2.5 and 5.0 min after the drop of 50 µL of a 10 µM MDMA solution in PBS (pH 7.4).

2.2.3 MN sensor fabrication, functionalization, and characterization
Firstly, the electrochemical cell was manufactured on a HMN array (**Fig. 1b - M1**). For that, the RE was first manually built by filling 5 MNs with a spatula using Ag/AgCl commercial paste and subsequently cured for 10 min at 70°C. Then, the WE and CE were built by filling 8 MNs and 12 MNs, respectively, using graphite commercial paste, and were again cured for 10 min at 70°C (the design is depicted in **Fig. 1b**). For each filling step, before curing, the excess paste was removed from the surface of the MNs using a scalpel, since the electrodes are meant to cover only the inside of the MNs. Separately, three connections (one for each electrode) were manually screen-printed on a PET substrate using silver paste and cured for 10 min at 100°C (**Fig. 1b - M5**).
The surface of the MN WE was functionalized by drop-casting a volume of 0.5 µL nanomaterial solution on each MN of the WE of the MN platform. Subsequently, the MN platform was dried at 70°C for 10 min. This process was repeated three times (the functionalization protocol was skipped for the preparation of the unmodified MN sensors). Afterward, the MN sensor was fixed on the connections using double adhesive tape and silver paste (to establish the connection between the RE, CE and WE to each correspondent connection). The assembly was subsequently cured for 10 min at 70°C. The area surrounding the MN platform was isolated using glue. The obtained platform was kept at room temperature for at least 12 hours. Finally, 10 cycles of CV from 0.3 V to 1.2 V with 100 mV s^{-1} in PBS (pH 7.4) were applied, after which the obtained MN sensor was rinsed with water (five times with 200 µL) and dried at 70°C for 10 min. A schematic representation of the fabrication process is depicted in **Fig. 1b**. At the beginning of each electrochemical experiment before testing the solution of interest, at least one blank test (i.e. SWV) was performed in PBS (pH 7.4) or AISF.
CVs were performed for the electrochemical characterization of the bare and nanomaterial-modified MN sensor in 5 mM $[Fe(CN)_6]^{4-/3-}$ solution in 0.1 M KCl (in the window of potential from -0.5 V to 1.2 V with a scan rate of 100 mV/s), and for the investigation of the MDMA electrochemical behavior on both sensors from a 100 µM MDMA solution in (PBS pH 7.4) (in the window of potential from -0.5 V to 1.2 V with a scan rate of 100 mV/s).

2.2.4 Analytical characterization of the MN sensor
The analytical performance of the MN sensor was evaluated by drop-casting 100 µL working solution on the surface of the sensor. Hence, MDMA solutions of increasing concentrations (1.0, 2.5, 5.0, 7.5, 10.0, 15.0, 25.0, 50.0 µM) were investigated by SWV in PBS (pH 7.4) using both the bare and the nanomaterial functionalized MN sensor. The obtained oxidation currents were plotted against the corresponding concentrations to build the calibration curves, based on which the sensitivity, LOD and LOQ were determined. The sensitivity was considered the slope of the calibration curve, while LOD and LOQ were calculated according to the following formulas: $LOD = 3.3*(S_y/S)$, $LOQ = 10*(S_y/S)$, where S_y is the standard deviation of the response and S is the slope of the calibration curve within the range from 1 to 25 µM.
Selectivity studies were performed in PBS (pH 7.4) by testing single solutions of the interferents (200 µM uric acid, 100 µM tyrosine, glycine, ascorbic acid, and 50 µM butylone,

3-methylmethcathinone, heroin, morphine, cocaine, benzoylecgonine, caffeine, paracetamol) and their binary mixtures with MDMA (10 µM and 50 µM).
Furthermore, the MDMA solutions of increasing concentration were interrogated in AISF at room temperature and at 33°C to assess the influence of the matrix and temperature over the performance of the MN sensor. Given the fact that the sensor is meant to pierce the skin, a parafilm piercing test was also performed to assess the robustness of the sensor after this simulated scenario. Parafilm M® has been proposed as a suitable alternative to the use of biological tissue, such as neonatal porcine skin, for MN array insertion studies [54]. The parafilm piercing test consists of performing a calibration curve before and after the insertion in the Parafilm M®. The parafilm piercing test was executed by pressing the MN sensor onto the Parafilm M® layers (8 × 127 µm) through a simple application of thumb pressure with the MNs tips piercing through the film layers, as previously reported [54]. Moreover, stability and reversibility tests were performed in AISF by testing the sensor in 10 and 50 µM MDMA solution every 30 min for 9h, and, respectively, by varying the concentration between 10 and 50 µM nine times.

3. Results and discussion

3.1 Design of the MN-based electrochemical sensor

In this work, a HMN array, as a minimally-invasive platform, has been integrated for the first time into an electrochemical sensor for the detection of MDMA in ISF. As a first step, an electrochemical cell was constructed on the HMN array by filling the holes of the MNs with conductive pastes (Ag/AgCl for the RE - 5 MNs and graphite paste for the CE - 8 MNs and WE - 12 MNs; **Fig. 1b**). An important detail here is the removal of the excess of paste on the outside surface of the MNs to avoid mechanical damage of the electrodes upon piercing. To evaluate the morphology of the modified HMN array with conductive pastes, scanning electron microscopy was employed. **Fig. S1** depicts the SEM images of the modified MNs and the corresponding electrode surfaces. **Fig S1A** shows the top view of a HMN modified with Ag/AgCl as the RE. The zoom into the electrode's surface exhibits the particulate shape of the Ag/AgCl pastes (**Fig S1B** and **Fig S1C**). **Fig. S1D** illustrates the top view of the carbon paste-modified HMN. The zoom into the electrode surface shows the wrinkled surface typical of commercial carbon-based SPEs (**Fig S1E** and **Fig S1F**) [58]. Thereafter, the fabricated electrochemical MN sensor was attached to a screen-printed connection (**M4** in **Fig. 1b**) through the cured paste located at the back of the patch (**Fig. 1b.II**). This connection enables a user-friendly insertion into a portable potentiostat. Importantly, the front side of the array maintained its ability to penetrate the skin (which was evaluated here through a parafilm piercing test - see *Section 3.4* - and elsewhere on pork skin [41,56]) and reach the ISF through the MN-based electrodes. Thus, the electrochemical detection of the species within the ISF can be performed after their diffusion towards the surface of the electrodes.
Prior to the MN platform fabrication, the selection of an optimal nanomaterial to functionalize the WE for increased sensitivity and improved LOD at physiological pH (7.4) was assessed. The nanomaterial may increase the electroactive surface area and potentially catalyzes the electrooxidation of MDMA at the surface of the WE. Hence, the influence of several nanomaterials over the electrochemical signal of MDMA was evaluated on SPEs. For this, the signal of a 10 µM MDMA solution was recorded on bare and modified (with SWCNTs, rGO, SDS, nD, AuNPs and PdNPs) SPEs. As can be observed in **Fig. 2a**, the highest peak current intensity (I_p) registered was on the SWCNTs-SPEs (0.7 µA), followed by the reduced GO (rGO; 0.22 µA, **Fig. 2b**) obtained from the GO after the reduction CV applied as described in the modification protocol, and the SDS-SPEs (0.6 µA, **Fig. 2c**). Furthermore, in these cases, a cathodic shift of the MDMA oxidation peak was observed, from 0.98 V on the bare SPEs to 0.91 V, 0.90 V and 0.90 V on the SWCNTs-, SDS- and rGO- SPEs. In the case of SWCNTs-SPEs and rGO-SPEs, this could be due to the higher working surface and increased conductivity provided by the two carbon-based nanomaterials, as previously reported for other illicit drugs as well [48,49]. The effect of SDS is most probably due to its surfactant properties, ensuring higher concentrations of the analyte at the interface between the electrode and

solution through two processes: (i) facilitating the adsorption of MDMA at the electrode surface (as previously reported [10] for other illicit drugs), and (ii) reducing the hydrophobicity of the electrode surface (as described for other surfactants as well [48]). Since both SWCNTs and GO solutions used for the modification contain surfactants for stabilization, the effect produced by the nanomaterials is most probably aided by the presence of the surfactant.
The nD particles generated a decrease of the MDMA signal from 0.1 µA on the bare SPEs to 0.05 µA on the nD-SPEs and an anodic shift of the peak potential (E_p) from 0.98 V to 1.01 V, respectively (**Fig. 2d**). Various concentrations of nD were investigated since it was previously reported that this could have an important influence on the signal enhancement [59]. It was suggested that rather lower concentrations of nDs had an amplifying effect over the I_p (at least in the case of the investigated analytes, dopamine and uric acid), while high concentrations of nDs could block the surface of the WE, forming a non-conductive layer. Nevertheless, in our case, an improvement over the MDMA signal was not obtained using nDs. A similar result was obtained when the PdNPs were used (**Fig. 2e**), the signal of MDMA being completely suppressed or shifted outside of the working window of potential. Lastly, when AuNPs-SPEs were explored, a signal in the blank was obtained in the same region as the MDMA oxidation peak (**Fig. 2f**), rendering this nanomaterial unsuited for MDMA detection.

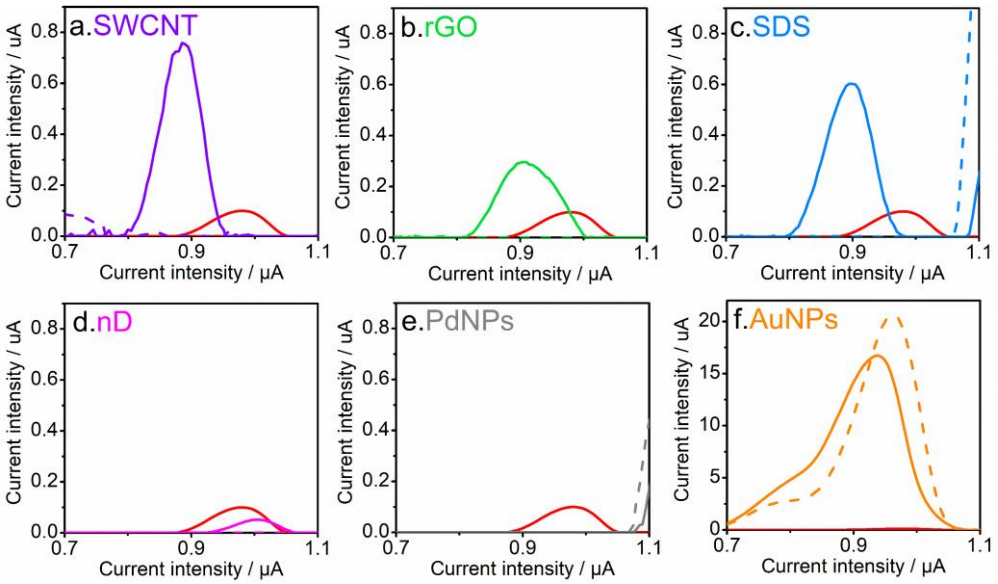

Fig. 2. Baseline corrected SWVs of MDMA 0 µM (blanks; dashed lines) and 10 µM (continuous lines) in buffer (PBS pH 7.4) on bare SPE (red lines, a-f), and SPE modified with (a) single-walled carbon nanotubes (SWCNT; purple lines), (b) reduced graphene oxide (rGO; green lines), (c) sodium dodecyl sulfate (SDS; blue lines), (d) nanodiamond particles (nD; pink lines), (e) palladium nanoparticles (PdNPs; grey lines) and (f) gold nanoparticles (AuNPs; yellow lines).

The influence of the accumulation time (the time of maintaining the solution on the surface of the sensor before analysis) on the electrochemical oxidation of bare, rGO-, SDS-, and SWCNTs-SPEs was subsequently evaluated. The increasing waiting time had no effect when the bare SPEs were investigated (**Fig. S2a**) but generated an increment in the peak current of MDMA in the case of SDS and nanomaterial-modified SPEs, hinting toward an adsorption-controlled phenomenon when using nanomaterials. From our previous works, a diffusion-controlled phenomenon governed the MDMA electrooxidation at bare electrodes [60], and an adsorption-controlled phenomenon occurred when using SDS [10]. The increase of the current intensity stopped after 2.5 min accumulation time in the case of rGO-SPEs (**Fig. S2b.ii**). Importantly, for the same waiting time, higher values of MDMA I_p were obtained on the SWCNTs-SPEs (**Fig. S2c.ii**) than on the rGO- and SDS-SPEs (e.g., 2.0 µA, 1.22 µA and 1.07 µA after 2.5 min, respectively). Furthermore, an anodic shift of the MDMA E_p was observed

with the increase of the waiting time when rGO-SPEs were tested (**Fig. S2b.iii**), while in the case of SDS- and SWCNTs-SPEs the E_p remained constant (**Fig. S2c.iii**). Nevertheless, after 2.5 min, the E_p remained constant on the rGO-SPEs as well. This is important since one of the previewed applications of the final sensor is to monitor the MDMA concentration in time, hence it is advantageous for the E_p to remain constant since its shift could make the data interpretation more complicated or even generate overlapping with other species present in the sample. Having these results, SWCNTs, one of the carbon-based nanomaterials, were selected for the surface functionalization of the MN sensor. Besides, the previewed application of the MN sensor includes the detection of intoxications with MDMA which are usually emergencies and require fast responses, thus an accumulation time of 2.5 min before analysis was chosen.

3.2 Evaluation of the electrochemical behavior of the MN sensor for MDMA electrooxidation

The bare and SWCNTs-modified MN (SWCNTs-MN) sensors, prepared as described in *Section 2.2.3*, were investigated by CV in 5 mM $[Fe(CN)_6]^{4-/3-}$ to evaluate the impact of the SWCNTs over the electrochemical performance of the MN platform. The registered CVs showed the reversible redox processes of the $[Fe(CN)_6]^{4-/3-}$ redox couple on both platforms (the corresponding values of the oxidation and reduction peaks on each platform are shown in **Fig. 3a**). Moreover, an increase in the capacitive current of the platform modified with SWCNTs was observed. Nevertheless, the current corresponding to the $[Fe(CN)_6]^{4-/3-}$ redox couple increased in intensity for both the oxidation peak (from 8.09 µA on the bare MNs to 19.05 µA on the SWCNTs-MNs) and the reduction peak (from -8.54 µA on the bare MNs to -16.54 µA on the SWCNTs-MNs). Furthermore, the oxidation peak of the redox couple registered a cathodic shift (of 120 mV), while the reduction peak registered an anodic shift (of 290 mV) on the SWCNTs-MN sensor, reducing the distance between the oxidation and reduction peaks by 410 mV. These changes suggest an improvement of the electron transfer rate on the SWCNTs MN platform, compared to the unmodified one. These findings are in agreement with the previously reported effects of the carbon nanotubes over the properties of other electrochemical platforms [48,49].

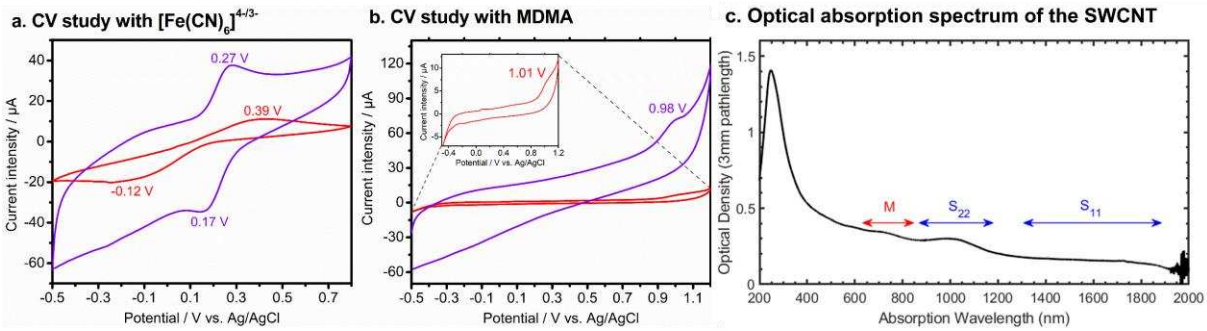

Fig. 3. *CV characterization (a and b) of the bare (red) and CNTs – modified (purple) MNs platforms in 5 mM [Fe(CN)6]$^{4-/3-}$ solution in 0.1 M KCl (a) and of 100 µM MDMA in PBS (pH 7.4) (b; inset: rescaled representation of the cyclic voltammogram on bare MN). (c)* Optical absorption spectrum of the SWCNT sample measured in a quartz cell with pathlength 3 mm. The arrows indicate the expected absorption ranges of the optical transitions of the semiconducting (S_11 and S_22, in blue) and metallic (M, in red) SWCNTs present in the sample.

The electrochemical behavior of MDMA was investigated on the bare and SWCNTs-MN sensors by SWV. **Fig. 3b** displays the irreversible oxidation of MDMA (to 3,4 - dihydroxy-methamphetamine [60]) from a 100 µM solution in PBS (pH 7.4) on both platforms: E_p=1.01 V on the bare MN sensor and E_p=0.98 V on the SWCNTs-MN sensor. Similarly to the effects observed for the 5 mM $[Fe(CN)_6]^{4-/3-}$ solution, a higher capacitive current, an increase in the

current intensity (of 3.9 μA) and a cathodic shift (of 30 mV) of the MDMA E_p, was observed when the SWCNTs were present on the MNs surface. Hence, the enhancement of the electron transfer rate manifested for MDMA on the SWCNTs-MN sensor as well. According to previously reported findings, this enhancement could be attributed to both the SWCNTs [48,49] as well as the surfactant [10] (as explained in *Section 3.1*) present in the solution used for the MNs modification. The very low optical density in the range of the S_11 transitions observed on the absorption spectra of the SWCNTs sample (**Fig. 3c**) is indicative of the doping of the SWCNTs in the aqueous surfactant solution.

3.3 Analytical performance in buffer

First, the electrochemical response in MDMA solutions of increasing concentration (between 1 μM and 50 μM) on both the bare and the SWCNTs-MN sensors in buffer was performed by SWV, with a 2.5 min accumulation time before analysis. The electrochemical oxidation of MDMA could be observed on both sensors, at an average value of 1.02 V (RSD=0.3% among the different concentrations, N=15) and 0.95 V (RSD=0.4% among the different concentrations, N=24) on the bare (**Fig. 4a**) and SWCNTs modified (**Fig. 4b**) MN sensors, respectively. Ergo, a cathodic shift (70 mV) of the MDMA peak occurred when SWCNTs were deposited on the surface of the WE. This shift is in accordance with the results obtained on the SWCNTs-SPEs (see *Section 3.1*) as well as previously reported work on the CNTs-modified electrodes [48,49]. When the bare MN sensor was used, a linear dependence of the I_p was obtained in the concentration range between 7.5 μM and 50 μM (**Fig. 4a**), described by the equation I_p (μA) = 0.004*[MDMA] (μM) - 0.03 (R^2=0.998; mean RSD of 12%, N=3 per each concentration), with a LOD of 8.3 μM and a LOQ of 25.7 μM. When the SWCNTs-MN sensor was employed, the interrogation of the SWCNTs-MN sensor between 1 μM and 50 μM showed a LOD and LOQ of 1.87 μM and 5.67 μM, respectively, making the SWCNTs-MN sensor suitable for MDMA detection in ISF (**Fig. 4b**). The reported concentrations of MDMA in the blood (therefore in ISF) are between 0.24 μM and 2.41 μM [32–34]. Furthermore, the linear dependence is described by the equation Ip (μA) = 0.0459*[MDMA] (μM) - 0.03 (R^2=0.998; mean RSD of 8%, N=3 per concentration), displaying an approximately 11 times higher sensitivity for the SWCNTs-MN sensor compared to the unmodified one (0.0459 μA μM^{-1} and 0.004 μA μM^{-1}, respectively). These results exhibit the superior performance of the SWCNTs-MN sensor for the detection of MDMA at physiological pH. Consequently, all the following experiments were performed using this functionalized sensor.

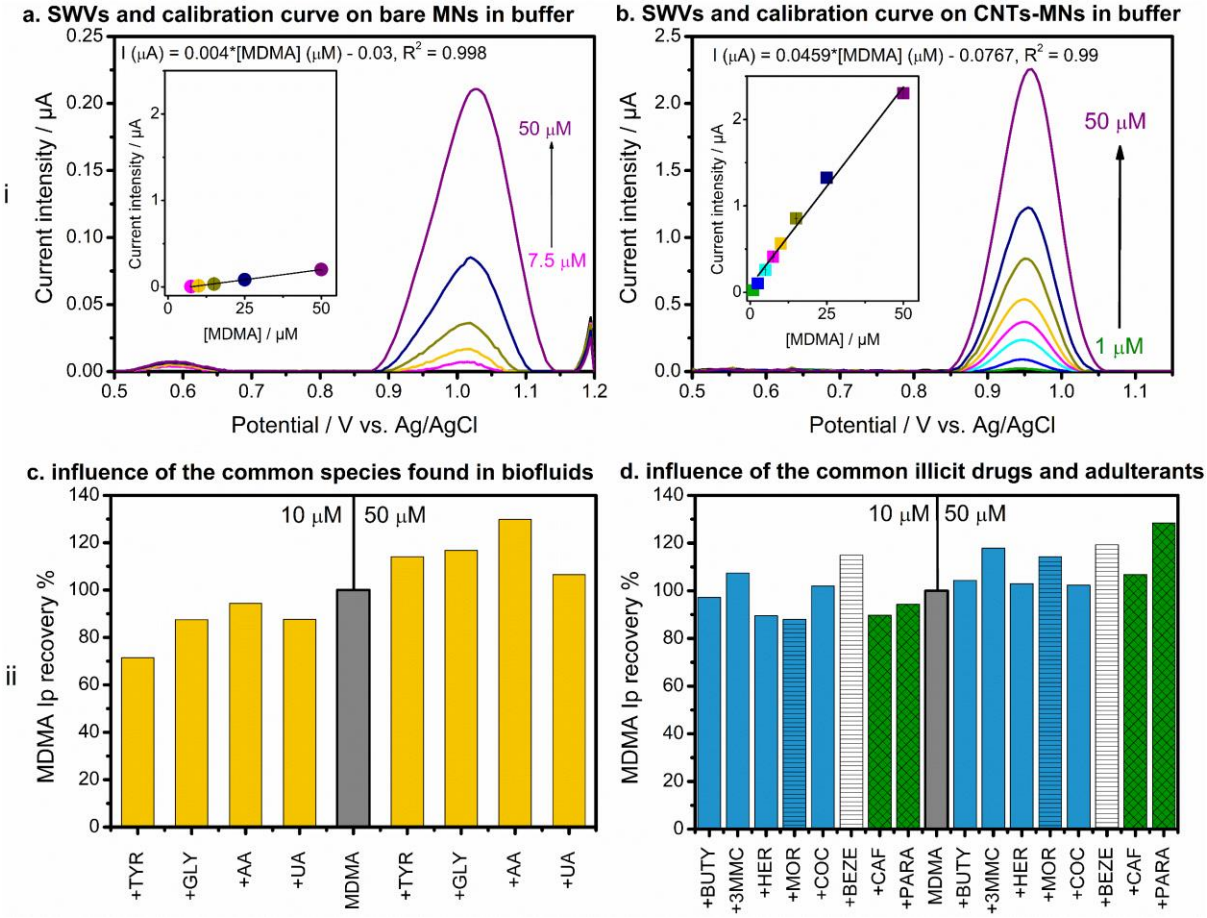

Fig. 4. *Analytical performance of the MN sensing platform for the detection of MDMA in buffer (PBS, pH 7.4): (i) SWVs of increasing concentrations of MDMA solutions from 7.5 μM to 50 μM using the bare MN sensor (a) and from 1 μM to 50 μM using the SWCNTs-MN platform (b); Insets: calibration curves obtained with the bare MN sensor (a) and SWCNTs-MN sensor (b) over the corresponding concentration ranges (equations displayed above the inset graphs); (ii) The influence of several molecules over the MDMA signal (grey column) at two levels of concentration for MDMA (10 μM on the left and 50 μM on the right side of the grey column) on the SWCNTs-MN in binary mixtures with: (c) common species found in biofluids (yellow columns): tyrosine – TYR, glycine – GLY, ascorbic acid – AA, uric acid – UA), (d) other common illicit drugs (blue columns), illicit drugs metabolites (stripes grided columns) and common adulterants (rhombi grided green columns): butylone – BUTY, 3-methylmethcathinone – 3MMC, heroine – HER, morphine - MOR, cocaine – COC, benzoylecgonine – BEZE, caffeine – CAF, paracetamol – PARA.*

The selectivity of the SWCNTs-MN sensor was evaluated in solutions of common species found in biofluids (uric acid, tyrosine, glycine, ascorbic acid [41]) as well as commonly abused illicit drugs (butylone, 3-methylmethcathinone, heroin, morphine, cocaine [3]), illicit drugs metabolites (morphine from heroin [51], benzoylecgonine from cocaine [52]) and frequently encountered adulterants (caffeine and paracetamol), separately and in binary mixtures with MDMA at two concentration levels of the target (10 μM and 50 μM; further details can be found in *Subsection 2.2.3*). **Fig. S3** depicts that the only electrochemically active molecules in the investigated window of potential in PBS (pH 7.4) were tyrosine, uric acid, heroin, morphine, and paracetamol. Nevertheless, their oxidation peaks occurred at 0.62 V, 0.33 V, 0.43 V, 0.41 V and 0.34 V, respectively, thus assuring an excellent separation from the MDMA peak (Ep=0.95 V). Binary mixtures of MDMA with these interferents were also evaluated and it can be observed that the investigated molecules did not shift the oxidation peak of MDMA (**Fig. S3**). The recoveries of the MDMA I_p were calculated based on the obtained I_p for MDMA in

pure solution and in binary mixtures with the interferants (the results are displayed in **Fig. 4c and 4d)**. Some variation over the current intensity of MDMA was registered, with recovery values between 71.4 % - 114.9 % and 102.3 % - 129.8 % for the 10 µM and 50 µM MDMA concentration levels, respectively. For the mixtures containing common species found in biofluids, a reduction in the MDMA signal between 5% and 13% was observed for the low-concentration level mixtures, except for the mixture with tyrosine (one of the electroactive compounds) when a reduction of 28% was observed. For the high-concentration mixtures, an increase of the MDMA signal was observed between 6% and 17% for all mixtures, except the mixture with ascorbic acid for which an increase of ~30% was observed.
For the mixtures containing other illicit drugs or their metabolites, variable modifications of the MDMA signal were observed for the low concentration level mixtures (in all cases under 15%): an increase was observed for the mixtures with butylone, heroin and morphine, the other generating a decrease in the MDMA signal. For the high concentration level mixtures, an increase of the MDMA signal between 5% and 23% was observed for all mixtures, except for the mixture with paracetamol when an increase of ~32% was obtained.
It is worth mentioning that some of the variations might be due to the manual preparation and modification of the sensor (a mean RSD of 8%, N=3 per concentration, was obtained during the calibration step as previously mentioned). Besides, it is suggested that working at low volumes on the MN sensor can potentially lead to evaporation effects, and thus an increment in the variability of the electrochemical signal.

3.4 Analytical performance in AISF

The designed SWCNTs-MN sensor is meant to be used as a wearable device for MDMA identification and monitoring in ISF. Therefore, the evaluation of the SWCNTs-MN sensor was addressed in AISF to emulate the closest conditions to the real scenario. Consequently, the electrochemical response of increasing concentrations of MDMA in AISF was evaluated in the same conditions as for the experiments in the buffer. **Fig. 5a and 5b** display the comparison of the SWVs and corresponding calibration curves obtained in the two media.

The two linear trendlines are superposable, presenting very similar slopes (0.0459 µA μM^{-1} in PBS and 0.0485 µA μM^{-1} in AISF with a mean RSD of 6%, N=3 per concentration), the LOD and LOQ for the analysis in AISF being 0.75 µM and 2.28 µM, respectively. It is important to mention that a slight anodic shift (of 5 mV) of the MDMA oxidation potential was observed in AISF, which can be attributed to the manual manufacturing process and is thus considered negligible for the analytical purpose. Another important parameter to consider for the successful analysis of MDMA in ISF using the SWCNTs-MN sensor is its mechanical resistance while penetrating the skin. Previously reported works have already shown the resistance of the HMN array after penetration in porcine skin [41,56]. Therefore, we evaluated the SWCNTs-MN electrochemical performance in AISF after its insertion into 8 layers (127 µm each) of Parafilm M®. **Fig. 5c** displays the perforation of the Parafilm M® by the MN during the parafilm piercing test. **Fig. 5d** exhibits the obtained calibration curve after the piercing test compared to the calibration curve obtained in AISF before the parafilm piercing test. Importantly, the linear dependence of the Ip on the MDMA concentration as well as the sensitivity remained unchanged. Consequently, we can affirm that the analytical performance of the SWCNTs-MN sensor was not affected by the parafilm piercing test, showing optimal mechanical resistance, and therefore, potentially suitable for skin penetration.

Wearable devices are normally skin-worn. Therefore, we evaluated the response of the electrochemical SWCNTs-MN sensor in AISF in the same range of concentration (between 1 µM and 50 µM) at 33°C (the average local temperature at the surface of the skin [61]), and subsequently compared it to the calibration curve obtained at RT. **Fig. 5e** displays the amplifying effect that this temperature increase had over the MDMA electrochemical oxidation. The corresponding equation exhibited a slope ~1.9 times higher (i.e. 0.091 µA μM^{-1}) than the one obtained at RT (i.e. 0.048 µA μM^{-1}) in the same concentration window, proving the effect of temperature in the analytical response. This variation of the current intensity generated by

the temperature increment was reported before for MDMA [60]. Usually, skin temperature remains constant, thus the calibration curve for adequate prediction would need to be performed at skin temperature. However, the integration of a temperature sensor along with the MN-based electrochemical sensor could also be useful for the use of the device in outdoor environments where big temperature differences exist.

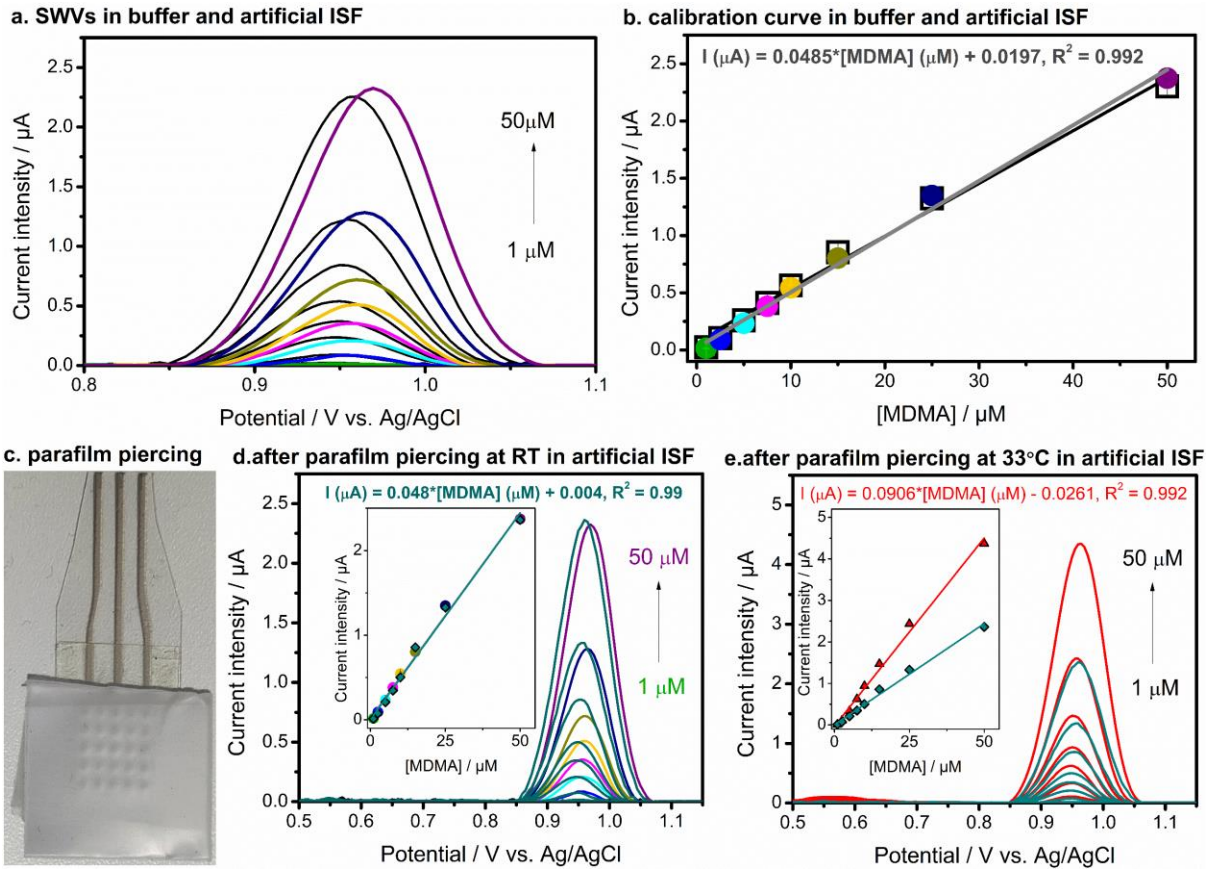

Fig. 5. *Analytical performance of the SWCNTs-MN sensor for the detection of MDMA in AISF in the concentration range from 1 μM to 50 μM: (a) SWVs and (b) calibration curves obtained at RT in PBS (black lines and squares, respectively) and in AISF (multi-colored lines and dots, respectively); (c) image of the Parafilm piercing test; (d) SWVs obtained at RT in AISF before (multi-colored lines) and after Parafilm piercing test (cyan lines); Inset: the calibration curves obtained in AISF at RT before (multi-colored dots) and after (cyan rhombi) the PPT; (e) SWVs obtained in AISF at RT (cyan lines) and 33°C (red lines); Inset: the calibration curves obtained in AISF at RT (cyan rhombi) and 33°C (red triangles).*

Lastly, reversibility and stability studies were performed in AISF to evaluate the ability of the device for continuous monitoring of MDMA fluctuations of concentration and for prolonged exposure times, respectively. The reversibility evaluation is necessary since the MDMA concentration in ISF is dynamic due to the pharmacokinetic processes occurring in the human body (absorption, distribution, metabolization and excretion). Therefore, the SWCNTs-MN sensor was tested by varying the MDMA concentration from 10 to 50 μM and back several times. In terms of Ip, a stable response was obtained for each concentration level with RDSs among the different measurements of 6.5 % and 2.1 % for the 10 μM and 50 μM solutions, respectively (**Fig. 6a**). Furthermore, for the Ep of the MDMA, RSDs of 0.26 % and 0.25% were registered, respectively (**Fig. 6b**), both parameters displaying the high reversibility of the system.

Finally, for the employment of the SWCNTs-MN sensor for MDMA monitoring in ISF, the assessment of the response stability is required over an extended period (e.g. several hours). Therefore, the response of the sensor was tested every 30 min for nine hours at two concentration levels (10 µM and 50 µM). Excellent RSD values were obtained for both the Ip (5.7 % and 2.8 %, respectively) and the E_p (0.2 % and 0.5 %), illustrating the high stability of the system in time.

Overall, the RSD values obtained for the reversibility and stability studies are similar to the RSD values obtained during the analytical characterization of the sensor. Hence, it can be affirmed that the SWCNTs-MN sensor displayed high reversibility and stability, meeting the required characteristics for MDMA identification and monitoring in ISF.

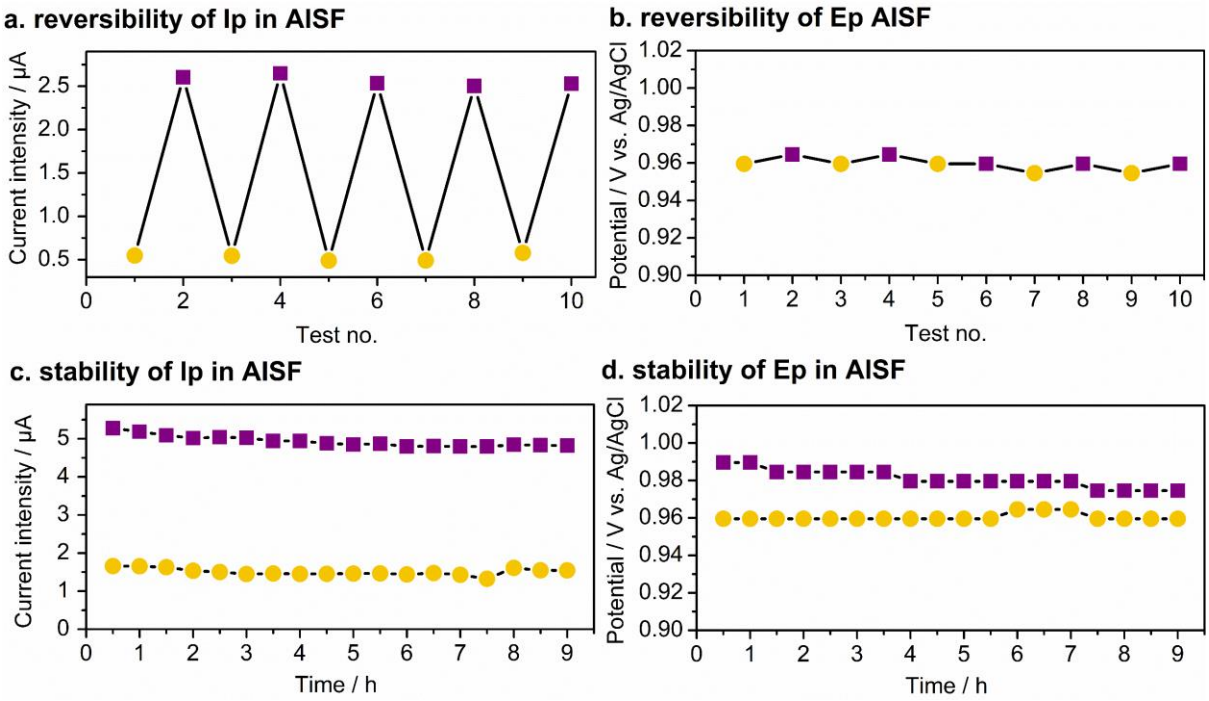

Fig. 6. *Investigation of the variation of the MDMA electrochemical signal in AISF at two concentration levels (10 µM – yellow dots and 50 µM – purple squares): reversibility study of the current intensity (Ip; a) and peak potential (Ep; b) by variation of concentration (e.g., from 10 µM to 50 µM to 10 µM, five tests/concentration), and stability study of the current intensity (c) and peak potential (d) by monitoring the response over an extended period (e.g., every 30 min. for nine hours) for each concentration.*

4. Conclusions

In this work, a SWCNTs functionalized HMN-based sensor was developed and tested for the electrochemical identification and monitoring of MDMA in ISF. We first developed a method for the fabrication of MN-based voltammetric sensors. Subsequently, we investigated the functionalization of the MN and the influence of the adsorption time upon the electrooxidation signal of MDMA. The study revealed that the use of the SWCNTs and 2.5 min accumulation time were the optimal parameters for the electrochemical detection of MDMA. Secondly, the analytical characterization of the SWCNTs-MN sensor was performed. The performance of this sensor was investigated in both buffer and AISF with excellent analytical features being observed, and importantly, fitting the detection limits necessary in case of MDMA consumption. Furthermore, the mechanical robustness of the sensor was evidenced by the piercing test maintaining the analytical capabilities. The sensor exhibited high selectivity, reversibility, and stability, making it suitable for the intended purpose.

It is important to mention that further optimization of the SWCNTs-MN sensor is needed since reaching sub-micromolar values remains a challenge for the detection of MDMA after several hours of consumption. Hence, we envision further improvements by the sorting of the nanotubes to only have metallic SWCNTs to increase the sensitivity of the system. Nevertheless, our MN sensor reached a sub-micromolar LOD with the concentration window potentially fitting MDMA levels in ISF. Besides, the employment of a coating is foreseen to avoid any potential leaking of the nanomaterials and to confer biocompatibility. Overall, we report a promising wearable patch for the minimally invasive monitoring of MDMA using an innovative SWCNTs-MN electrochemical system which could be employed to track drug consumers under probation and to monitor the therapeutic levels in patients undergoing MDMA treatment.

Credit author statement

Ana-Maria Drăgan: formal analysis, investigation (optimization, fabrication and assembly of the MN sensor, electrochemical and analytical characterization of the MN sensor), writing – original draft, visualization. **Marc Parrilla**: methodology, designing experiments, investigation (fabrication and assembly of the MN sensor), writing – review & editing. **Sofie Cambré**: provision of the carbon nanotubes and writing – review & editing. **Juan Domínguez-Robles**: writing – review & editing. **Usanee Detamornrat:** design of the hollow microneedle array. **Ryan F. Donnelly**: investigation (designing the HMN array) and writing – review & editing. **Radu Oprean**: writing – review & editing, supervision. **Cecilia Cristea and Karolien De Wael**: writing – review & editing, supervision, project administration. The manuscript was written through the contributions of all authors. All authors have approved the final version of the manuscript.

Declaration of competing interest

The authors declare that they have no known competing financial interests or personal relationships that could have appeared to influence the work reported in this paper.

Acknowledgments

The authors acknowledge the support of the European Union's Horizon 2020 Research and Innovation Programme under grant agreement No 833787, BorderSens. This work was also supported in part by EPSRC grant EP/H021647/1. A.-M. D acknowledges the support of the PhD Research Project no. 774/2/11.01.2023 offered by "Iuliu Haţieganu" University of Medicine and Pharmacy, Cluj-Napoca. M.P acknowledges the support of the Fund for Scientific Research (FWO) in Flanders (K217022N and 1265223N), Belgium. J.D.-R. acknowledges the financial support from the Ramón y Cajal grant RYC-2021-034357-I funded by MCIN/AEI/10.13039/501100011033 and by the "European Union NextGenerationEU/PRTR".

References

[1] A.-M. Dragan, M. Parrilla, B. Feier, R. Oprean, C. Cristea, K. De Wael, Analytical techniques for the detection of Amphetamine-type substances in different matrices: a comprehensive review, TrAC Trends Anal. Chem. 145 (2021) 116447. https://doi.org/10.1016/j.trac.2021.116447.

[2] European Monitoring Centre for Drugs and Drug Addiction, European Drug Report 2022: Trends and developments, 2022. https://doi.org/10.2810/715044.

[3] United Nations Office on Drugs and Crime - UNODC, United Nations Office on Drugs and Crime, World Drug Report 2022 - Booklet 2. Global Overview: Drug Demand Drug Supply, 2022.

[4] J. Welter-Luedeke, H.H. Maurer, New Psychoactive Substances: Chemistry, Pharmacology, Metabolism, and Detectability of Amphetamine Derivatives with Modified Ring Systems, Ther. Drug Monit. 38 (2016) 4–11. https://doi.org/10.1097/FTD.0000000000000240.

[5] A.G. Verstraete, T. Mukhdomi, Clinical Drug Testing, StatPearls Publishing, 2021.

[6] R. Dong, S. Weng, L. Yang, J. Liu, Detection and direct readout of drugs in human urine using dynamic surface-enhanced Raman spectroscopy and support vector machines, Anal. Chem. 87 (2015) 2937–2944. https://doi.org/10.1021/acs.analchem.5b00137.

[7] S. Weng, R. Dong, Z. Zhu, D. Zhang, J. Zhao, L. Huang, D. Liang, Dynamic surface-enhanced Raman spectroscopy and Chemometric methods for fast detection and intelligent identification of methamphetamine and 3, 4-Methylenedioxy methamphetamine in human urine, Spectrochim. Acta - Part A Mol. Biomol. Spectrosc. 189 (2018) 1–7. https://doi.org/10.1016/j.saa.2017.08.004.

[8] C. Pollard, M. Hudson, J.M. McDonnell, P.G. Royall, K. Wolff, Development of a point-of-care test for the detection of MDMA in latent fingerprints using surface plasmon resonance and lateral flow technology, Drug Test. Anal. 14 (2022) 613–621. https://doi.org/10.1002/dta.3196.

[9] É. Naomi Oiye, J. Midori Toia Katayama, M. Fernanda Muzetti Ribeiro, L. Oka Duarte, R. de Castro Baker Botelho, A. José Ipólito, B. Royston McCord, M. Firmino de Oliveira, Voltammetric detection of 3,4-methylenedioxymethamphetamine (mdma) in saliva in low cost systems, Forensic Chem. 20 (2020) 100268. https://doi.org/10.1016/j.forc.2020.100268.

[10] M. Parrilla, F. Joosten, K. De Wael, Enhanced electrochemical detection of illicit drugs in oral fluid by the use of surfactant-mediated solution, Sensors Actuators B Chem. 348 (2021) 130659. https://doi.org/10.1016/j.snb.2021.130659.

[11] D. Butler, M. Pravda, G.G. Guilbault, Development of a disposable amperometric immunosensor for the detection of ecstasy and its analogues using screen-printed electrodes, Anal. Chim. Acta. 556 (2006) 333–339. https://doi.org/10.1016/j.aca.2005.09.056.

[12] R.A.S. Couto, S.S. Costa, B. Mounssef, J.G. Pacheco, E. Fernandes, F. Carvalho, C.M.P. Rodrigues, C. Delerue-Matos, A.A.C. Braga, L. Moreira Gonçalves, M.B. Quinaz, Electrochemical sensing of ecstasy with electropolymerized molecularly imprinted poly(o-phenylenediamine) polymer on the surface of disposable screen-printed carbon electrodes, Sensors Actuators, B Chem. 290 (2019) 378–386. https://doi.org/10.1016/j.snb.2019.03.138.

[13] R. Zhang, K. Fu, F. Zou, H. Bai, G. Zhang, F. Liang, Q. Liu, Highly sensitive electrochemical sensor based on Pt nanoparticles/carbon nanohorns for simultaneous determination of morphine and MDMA in biological samples, Electrochim. Acta. 370 (2021) 137803. https://doi.org/10.1016/j.electacta.2021.137803.

[14] M. Navarro, S. Pichini, M. Farré, J. Ortuño, P.N. Roset, J. Segura, R. De La Torre, Usefulness of saliva for measurement of 3,4-methylenedioxymethamphetamine and its metabolites: Correlation with plasma drug concentrations and effect of salivary pH, Clin. Chem. 47 (2001) 1788–1795. https://doi.org/10.1093/clinchem/47.10.1788.

[15] E.M.P.J. Garrido, J.M.P.J. Garrido, N. Milhazes, F. Borges, A.M. Oliveira-Brett, Electrochemical oxidation of amphetamine-like drugs and application to electroanalysis of ecstasy in human serum, Bioelectrochemistry. 79 (2010) 77–83. https://doi.org/10.1016/j.bioelechem.2009.12.002.
[16] L. Lu, J. Zhang, Y. Xie, F. Gao, S. Xu, X. Wu, Z. Ye, Wearable Health Devices in Health Care: Narrative Systematic Review, JMIR MHealth UHealth. 8 (2020). https://doi.org/10.2196/18907.
[17] D. Rybak, Y.-C. Su, Y. Li, B. Ding, X. Lv, Z. Li, Y.-C. Yeh, P. Nakielski, C. Rinoldi, F. Pierini, J.M. Dodda, Evolution of nanostructured skin patches towards multifunctional wearable platforms for biomedical applications, Nanoscale. 15 (2023) 8044–8083. https://doi.org/10.1039/D3NR00807J.
[18] Z. Deng, L. Guo, X. Chen, W. Wu, Smart Wearable Systems for Health Monitoring, Sensors. 23 (2023) 2479. https://doi.org/10.3390/s23052479.
[19] H. Teymourian, M. Parrilla, J.R. Sempionatto, N.F. Montiel, A. Barfidokht, R. Van Echelpoel, K. De Wael, J. Wang, Wearable Electrochemical Sensors for the Monitoring and Screening of Drugs, ACS Sensors. 5 (2020) 2679−2700. https://doi.org/10.1021/acssensors.0c01318.
[20] R.K. Mishra, J.R. Sempionatto, Z. Li, C. Brown, N.M. Galdino, R. Shah, S. Liu, L.J. Hubble, K. Bagot, S. Tapert, J. Wang, Simultaneous detection of salivary Δ9-tetrahydrocannabinol and alcohol using a Wearable Electrochemical Ring Sensor, Talanta. 211 (2020) 120757. https://doi.org/10.1016/j.talanta.2020.120757.
[21] M. de Jong, N. Sleegers, J. Kim, F. Van Durme, N. Samyn, J. Wang, K. De Wael, Electrochemical fingerprint of street samples for fast on-site screening of cocaine in seized drug powders, Chem. Sci. 7 (2016) 2364–2370. https://doi.org/10.1039/C5SC04309C.
[22] A. Barfidokht, R.K. Mishra, R. Seenivasan, S. Liu, L.J. Hubble, J. Wang, D.A. Hall, Wearable electrochemical glove-based sensor for rapid and on-site detection of fentanyl, Sensors Actuators, B Chem. 296 (2019) 126422. https://doi.org/10.1016/j.snb.2019.04.053.
[23] R.K. Mishra, K.Y. Goud, Z. Li, C. Moonla, M.A. Mohamed, F. Tehrani, H. Teymourian, J. Wang, Continuous Opioid Monitoring along with Nerve Agents on a Wearable Microneedle Sensor Array, J. Am. Chem. Soc. 142 (2020) 5991–5995. https://doi.org/10.1021/jacs.0c01883.
[24] P. Tullis, How ecstasy and psilocybin are shaking up psychiatry, Nature. 589 (2021) 506–509. https://doi.org/10.1038/d41586-021-00187-9.
[25] C.M. Reiff, E.E. Richman, C.B. Nemeroff, L.L. Carpenter, A.S. Widge, C.I. Rodriguez, N.H. Kalin, W.M. McDonald, Psychedelics and psychedelic-assisted psychotherapy, Am. J. Psychiatry. 177 (2020) 391–410. https://doi.org/10.1176/APPI.AJP.2019.19010035/ASSET/IMAGES/LARGE/APPI.AJP.2019.19010035F1.JPEG.
[26] C. Rodriguez, MDMA-Assisted Cognitive Behavioral Therapy (CBT) Compared With Methamphetamine-Assisted CBT in Obsessive-Compulsive Disorder (OCD): A Phase II Study (NCT05783817), (2023).
[27] A.L. Danforth, C.S. Grob, C. Struble, A.A. Feduccia, N. Walker, L. Jerome, B. Yazar-Klosinski, A. Emerson, Reduction in social anxiety after MDMA-assisted psychotherapy with autistic adults: a randomized, double-blind, placebo-controlled pilot study, Psychopharmacology (Berl). 235 (2018) 3137–3148. https://doi.org/10.1007/S00213-018-5010-9.
[28] P.E. Wolfson, J. Andries, A.A. Feduccia, L. Jerome, J.B. Wang, E. Williams, S.C. Carlin, E. Sola, S. Hamilton, B. Yazar-Klosinski, A. Emerson, M.C. Mithoefer, R. Doblin, MDMA-assisted psychotherapy for treatment of anxiety and other psychological distress related to life-threatening illnesses: a randomized pilot study, Sci. Rep. 10 (2020) 20442. https://doi.org/10.1038/s41598-020-75706-1.
[29] J.M. Mitchell, M. Bogenschutz, A. Lilienstein, C. Harrison, S. Kleiman, K. Parker-Guilbert, M. Ot'alora G, W. Garas, C. Paleos, I. Gorman, C. Nicholas, M. Mithoefer, S.

Carlin, B. Poulter, A. Mithoefer, S. Quevedo, G. Wells, S.S. Klaire, B. van der Kolk, K. Tzarfaty, R. Amiaz, R. Worthy, S. Shannon, J.D. Woolley, C. Marta, Y. Gelfand, E. Hapke, S. Amar, Y. Wallach, R. Brown, S. Hamilton, J.B. Wang, A. Coker, R. Matthews, A. de Boer, B. Yazar-Klosinski, A. Emerson, R. Doblin, MDMA-assisted therapy for severe PTSD: a randomized, double-blind, placebo-controlled phase 3 study, Nat. Med. 27 (2021) 1025–1033. https://doi.org/10.1038/S41591-021-01336-3.

[30] L. Ponte, L. Jerome, S. Hamilton, M.C. Mithoefer, B.B. Yazar-Klosinski, E. Vermetten, A.A. Feduccia, Sleep Quality Improvements After MDMA-Assisted Psychotherapy for the Treatment of Posttraumatic Stress Disorder, J. Trauma. Stress. 34 (2021) 851–863. https://doi.org/10.1002/JTS.22696.

[31] Therapeutic Goods Administration, Change to classification of psilocybin and MDMA to enable prescribing by authorised psychiatrists, 3 (2023) 9–11.

[32] H.J. Helmlin, K. Bracher, D. Bourquin, D. Vonlanthen, R. Brenneisen, J. Styk, Analysis of 3,4-methylenedioxymethamphetamine (MDMA) and its metabolites in plasma and urine by HPLC-DAD and GC-MS, J. Anal. Toxicol. 20 (1996) 432–440. https://doi.org/10.1093/jat/20.6.432.

[33] R.L. Hartman, N.A. Desrosiers, A.J. Barnes, K. Yun, K.B. Scheidweiler, E.A. Kolbrich-Spargo, D.A. Gorelick, R.S. Goodwin, M.A. Huestis, 3,4-Methylenedioxymethamphetamine (MDMA) and metabolites disposition in blood and plasma following controlled oral administration, Anal. Bioanal. Chem. 406 (2014) 587–599. https://doi.org/10.1007/s00216-013-7468-y.

[34] N. Pizarro, J. Ortuno, M. Farre, C. Hernandez-Lopez, M. Pujadas, A. Llebaria, J. Joglar, P.N. Roset, M. Mas, J. Segura, J. Cami, R. de la Torre, Determination of MDMA and its Metabolites in Blood and Urine by Gas Chromatography-Mass Spectrometry and Analysis of Enantiomers by Capillary Electrophoresis, J. Anal. Toxicol. 26 (2002) 157–165. https://doi.org/10.1093/jat/26.3.157.

[35] P. Mao, H. Li, Z. Yu, A Review of Skin-Wearable Sensors for Non-Invasive Health Monitoring Applications, Sensors (Basel). 23 (2023) 3673. https://doi.org/10.3390/S23073673.

[36] M. Friedel, I.A.P. Thompson, G. Kasting, R. Polsky, D. Cunningham, H.T. Soh, J. Heikenfeld, Opportunities and challenges in the diagnostic utility of dermal interstitial fluid, Nat. Biomed. Eng. (2023). https://doi.org/10.1038/s41551-022-00998-9.

[37] H. Sun, Y. Zheng, G. Shi, H. Haick, M. Zhang, Wearable Clinic: From Microneedle-Based Sensors to Next-Generation Healthcare Platforms, Small. (2023). https://doi.org/10.1002/smll.202207539.

[38] J. Heikenfeld, A. Jajack, B. Feldman, S.W. Granger, S. Gaitonde, G. Begtrup, B.A. Katchman, Accessing analytes in biofluids for peripheral biochemical monitoring, Nat. Biotechnol. 37 (2019) 407–419. https://doi.org/10.1038/s41587-019-0040-3.

[39] L. Zhao, C. Zhang, J.M. Abu-Ershaid, M. Li, Y. Li, Y. Naser, X. Dai, M.T.A. Abbate, R.F. Donnelly, Smart Responsive Microarray Patches for Transdermal Drug Delivery and Biological Monitoring, Adv. Healthc. Mater. 10 (2021) 2100996. https://doi.org/10.1002/adhm.202100996.

[40] S. Ma, J. Li, L. Pei, N. Feng, Y. Zhang, Microneedle-based interstitial fluid extraction for drug analysis: Advances, challenges, and prospects, J. Pharm. Anal. 13 (2023) 111–126. https://doi.org/10.1016/j.jpha.2022.12.004.

[41] M. Parrilla, U. Detamornrat, J. Domínguez-Robles, R.F. Donnelly, K. De Wael, Wearable Hollow Microneedle Sensing Patches for the Transdermal Electrochemical Monitoring of Glucose, Talanta. 249 (2022) 123695. https://doi.org/10.1016/j.talanta.2022.123695.

[42] X. Li, X. Huang, J. Mo, H. Wang, Q. Huang, C. Yang, T. Zhang, H.J. Chen, T. Hang, F. Liu, L. Jiang, Q. Wu, H. Li, N. Hu, X. Xie, A Fully Integrated Closed-Loop System Based on Mesoporous Microneedles-Iontophoresis for Diabetes Treatment, Adv. Sci. 8 (2021) 2100827. https://doi.org/10.1002/advs.202100827.

[43] F. Ribet, G. Stemme, N. Roxhed, Real-time intradermal continuous glucose monitoring using a minimally invasive microneedle-based system, Biomed.

Microdevices. 20 (2018) 101. https://doi.org/10.1007/s10544-018-0349-6.
[44] A.M.V. Mohan, J.R. Windmiller, R.K. Mishra, J. Wang, Continuous minimally-invasive alcohol monitoring using microneedle sensor arrays, Biosens. Bioelectron. 91 (2017) 574–579. https://doi.org/10.1016/j.bios.2017.01.016.
[45] K.Y. Goud, K. Mahato, H. Teymourian, K. Longardner, I. Litvan, J. Wang, Wearable Electrochemical Microneedle Sensing Platform for Real-Time Continuous Interstitial Fluid Monitoring of Apomorphine: Toward Parkinson Management, Sensors Actuators B Chem. 354 (2022) 131234. https://doi.org/10.1016/j.snb.2021.131234.
[46] M. Parrilla, A. Vanhooydonck, M. Johns, R. Watts, K. De Wael, 3D-printed microneedle-based potentiometric sensor for pH monitoring in skin interstitial fluid, Sensors Actuators B. Chem. 378 (2023) 133159. https://doi.org/10.1016/j.snb.2022.133159.
[47] E. Olesti, M. Farré, M. Carbó, E. Papaseit, C. Perez-Mañá, M. Torrens, S. Yubero-Lahoz, M. Pujadas, Ó.J. Pozo, R. de la Torre, Dose-Response Pharmacological Study of Mephedrone and Its Metabolites: Pharmacokinetics, Serotoninergic Effects, and Impact of CYP2D6 Genetic Variation, Clin. Pharmacol. Ther. 106 (2019) 596–604. https://doi.org/10.1002/CPT.1417.
[48] A.-M. Dragan, F.M. Truta, M. Tertis, A. Florea, J. Schram, A. Cernat, B. Feier, K. De Wael, C. Cristea, R. Oprean, Electrochemical Fingerprints of Illicit Drugs on Graphene and Multi-Walled Carbon Nanotubes, Front. Chem. 9 (2021) 1–10. https://doi.org/10.3389/fchem.2021.641147.
[49] F. Truta, A. Florea, A. Cernat, M. Tertis, O. Hosu, K. de Wael, C. Cristea, Tackling the Problem of Sensing Commonly Abused Drugs Through Nanomaterials and (Bio)Recognition Approaches, Front. Chem. 8 (2020) 1–18. https://doi.org/10.3389/fchem.2020.561638.
[50] I. Kim, J.M. Oyler, E.T. Moolchan, E.J. Cone, M.A. Huesitis, Urinary pharmacokinetics of methamphetamine and its metabolite, amphetamine following controlled oral administration to humans, Ther. Drug Monit. 26 (2004) 664–672. https://doi.org/10.1097/00007691-200412000-00013.
[51] E. Rook, A. Huitema, W. Brink, J. Ree, J. Beijnen, Pharmacokinetics and Pharmacokinetic Variability of Heroin and its Metabolites: Review of the Literature, Curr. Clin. Pharmacol. 1 (2008) 109–118. https://doi.org/10.2174/157488406775268219.
[52] R.A. Goldstein, C. DesLauriers, A. Burda, K. Johnson-Arbor, Cocaine: history, social implications, and toxicity: a review, Semin. Diagn. Pathol. 26 (2009) 10–17. https://doi.org/10.1053/J.SEMDP.2008.12.001.
[53] A. Żubrycka, A. Kwaśnica, M. Haczkiewicz, K. Sipa, K. Rudnicki, S. Skrzypek, L. Poltorak, Illicit drugs street samples and their cutting agents. The result of the GC-MS based profiling define the guidelines for sensors development, Talanta. 237 (2022) 122904. https://doi.org/10.1016/J.TALANTA.2021.122904.
[54] E. Larrañeta, J. Moore, E.M. Vicente-Pérez, P. González-Vázquez, R. Lutton, A.D. Woolfson, R.F. Donnelly, A proposed model membrane and test method for microneedle insertion studies, Int. J. Pharm. 472 (2014) 65–73. https://doi.org/10.1016/j.ijpharm.2014.05.042.
[55] C.D. Mendonça, S.U. Khan, V. Rahemi, S.W. Verbruggen, S.A.S. Machado, K. De Wael, Surface plasmon resonance-induced visible light photocatalytic TiO2 modified with AuNPs for the quantification of hydroquinone, Electrochim. Acta. 389 (2021). https://doi.org/10.1016/j.electacta.2021.138734.
[56] U. Detamornrat, M. Parrilla, J. Domínguez-Robles, Q.K. Anjani, E. Larrañeta, K. De Wael, R.F. Donnelly, Transdermal on-demand drug delivery based on an iontophoretic hollow microneedle array system, Lab Chip. 23 (2023) 2304–2315. https://doi.org/10.1039/D3LC00160A.
[57] M. Dervisevic, M. Alba, L. Yan, M. Senel, T.R. Gengenbach, B. Prieto-Simon, N.H. Voelcker, Transdermal Electrochemical Monitoring of Glucose via High-Density Silicon Microneedle Array Patch, Adv. Funct. Mater. 32 (2021) 2009850.

https://doi.org/10.1002/adfm.202009850.
[58] N. Felipe Montiel, M. Parrilla, V. Beltrán, G. Nuyts, F. Van Durme, K. De Wael, The opportunity of 6-monoacetylmorphine to selectively detect heroin at preanodized screen printed electrodes, Talanta. 226 (2021) 122005. https://doi.org/10.1016/j.talanta.2020.122005.
[59] M. Baccarin, S.J. Rowley-Neale, É.T.G. Cavalheiro, G.C. Smith, C.E. Banks, Nanodiamond based surface modified screen-printed electrodes for the simultaneous voltammetric determination of dopamine and uric acid, Microchim. Acta. 186 (2019) 1–9. https://doi.org/10.1007/s00604-019-3315-y.
[60] R. Van Echelpoel, M. Parrilla, N. Sleegers, S.T. Shanmugam, A.L.N. van Nuijs, A. Slosse, F. Van Durme, K. De Wael, Validated portable device for the qualitative and quantitative electrochemical detection of MDMA ready for on-site use, Microchem. J. 190 (2023) 108693. https://doi.org/10.1016/j.microc.2023.108693.
[61] W. Bierman, The temperature of the skin surface, J. Am. Med. Assoc. 106 (1936) 1158–1162. https://doi.org/10.1001/jama.1936.02770140020007.